Hyperfine structure and hyperfine coherent properties of praseodymium in single-crystalline $La_2(WO_4)_3$ by hole-burning and photon-echo techniques

O. Guillot-Noël,* Ph. Goldner, F. Beaudoux, Y. Le Du, and J. Lejay
Laboratoire de Chimie de la Matière Condensée de Paris, ENSCP, CNRS-UMR 7574, 11 rue Pierre et Marie Curie 75231 Paris Cedex 05, France

A. Amari, A. Walther, L. Rippe, and S. Kröll
Department of Physics, Lund Institute of Technology, P.O. Box 118, S-22100 Lund, Sweden
(Received 26 December 2008; published 27 April 2009)

We studied the hyperfine structure and hyperfine coherent properties of the $^3H_4(0) \rightarrow {}^1D_2(0)$ transition of Pr^{3+} ions in a tungstate single crystal $La_2(WO_4)_3$ by hole-burning and photon-echo techniques. This work is motivated by the search of an efficient three level Λ system in this new compound with which we could build up a quantum memory. By nonconventional hole-burning experiments, the ordering of the hyperfine splittings in the $^3H_4(0)$ ground state and in the $^1D_2(0)$ excited state is obtained. The hyperfine splittings are thus ordered: 24.6 and 14.9 MHz for the $^3H_4(0)$ level and 5.0 and 7.3 MHz for the $^1D_2(0)$ level. The relative and absolute transition strengths of individual hyperfine transitions are determined by comparing absorption strengths and by measuring the Rabi flopping frequency as the transition is coherently driven. Free induction and Raman echo decays give inhomogeneous and homogeneous hyperfine linewidths of 57 ± 2 and 1.25 ± 0.1 kHz, respectively.

DOI: 10.1103/PhysRevB.79.155119 PACS number(s): 42.50.Md, 42.62.Fi, 78.55.−m

I. INTRODUCTION

The storage and retrieval of a quantum state of light is expected to play a fundamental role in long distance quantum communication networks.[1–3] Storage was demonstrated for classical and quantum light in a number of systems.[4–8] For example, storage and retrieval of a single photon was implemented in a cloud of laser cooled atoms.[5] Rare earth ions in inorganic crystals (REIC) are promising candidates in the quest for macroscopic quantum effects and in particular in the areas of quantum computing[9,10] and quantum state storage.[11,12] Indeed, some rare-earth ions exhibit long-lived nuclear spin ground-state levels called hyperfine levels. These levels can be put into a coherent superposition for a long time and can potentially be used for storage of quantum information. At low temperature (1.5 K), a hyperfine coherence (T_2) lifetime >1 s was reported in $Pr^{3+}:Y_2SiO_5$ (Pr:YSO).[13] Moreover, rare-earth optical transitions can also exhibit a long coherence lifetime (up to 6.4 ms).[14]

Quantum state storage is commonly pursued with atomic species in which a three-level Λ system can be built.[15] A three-level Λ system consists of two levels, which can both be coupled to a third level using light fields. The photon to be stored is resonant with one transition and a second light field with the other one. Intensity variation in the latter, for example, allows photons to be trapped and released by using electromagnetically induced transparency (EIT) and slow light.[15] EIT, slow and stopped light were demonstrated in REIC.[8,11,16] In Pr:YSO, light was stopped for a time greater than 1 s.[11] In praseodymium-doped materials, the three-level Λ system is composed of two hyperfine levels, belonging to the ground $^3H_4(0)$ electronic level, which are optically connected to one hyperfine level within the excited $^1D_2(0)$ electronic level. Very recently, robust population transfer by stimulated Raman adiabatic passage was also obtained in the same Pr:YSO host.[17]

Most of the experiments involving REIC for quantum applications have so far been performed on yttrium orthosilicate single crystals. In a previous work,[18] we proposed a praseodymium oxide host: $Pr^{3+}:La_2(WO_4)_3$ for such applications. The hyperfine splittings, the optical inhomogeneous, and homogeneous linewidths of the $^3H_4(0) \rightarrow {}^1D_2(0)$ transition and the spectral-hole lifetime due to population redistribution within the ground hyperfine levels were studied in a 1.4% $Pr^{3+}:La_2(WO_4)_3$ compound. The results obtained in Ref. 18 indicate that this crystal could be an interesting host for quantum applications. Relevant parameters include an inhomogeneous linewidth of 18.8 GHz for a concentration of $1.09\ 10^{20}$ at/cm^3 and a hole lifetime of 16 s long enough to perform spectral selection.

To characterize the properties of a three-level Λ system in this new compound in order to assess its potential for quantum applications, a deeper study of the hyperfine characteristics of Pr^{3+} ions in the tungstate host needs to be performed. The ordering of the hyperfine levels in the ground $^3H_4(0)$ and $^1D_2(0)$ excited states, the relative and absolute oscillator strengths between individual hyperfine transitions, the inhomogeneous, and homogeneous hyperfine linewidth are relevant parameters for defining an efficient three-level system. The purpose of the present work is to measure these quantities. As the praseodymium hyperfine splittings (few tenths of MHz) are smaller than the inhomogeneous linewidth of the $^3H_4(0) \rightarrow {}^1D_2(0)$ transition (several tenths of GHz), such experiments are nontrivial. However, they can be done by preparing the optical inhomogeneous absorption profile so that the light only interacts with a narrow absorption from an ensemble of identical ions which all absorb on a specific hyperfine transitions at this frequency. After this preparation step, all of the required hyperfine characteristics can be measured by absorption and state-transfer techniques that include coherent manipulations of individual hyperfine transitions.

The paper is organized as follows. In Sec. II, the experimental apparatus is presented. In this section, the different excitation pulses used to prepare and to coherently drive the individual hyperfine transitions are explained. In Sec. III, the experimental results are presented and discussed. In the first part, the ordering of the hyperfine levels and the relative oscillator strengths are determined. In the second part, the oscillator strengths of these transitions are obtained by Rabi flopping. In the third part, the inhomogeneous and homogeneous hyperfine linewidths are measured by optically exciting a hyperfine coherence and by studying the induced hyperfine free induction decay (FID) and Raman echo, respectively.

II. EXPERIMENT

$Pr^{3+}:La_2(WO_4)_3$ single crystals were grown by the Czochralski method following the procedure explained in Ref. 19. Lanthanum tungstate crystal belongs to the monoclinic system with space group $C2/c$, with unit parameters $a=7.873(2)$ Å, $b=11.841(2)$ Å, $c=11.654(2)$ Å, $\beta=109.25(3)$, and $Z=4$.[20] Pr^{3+} ions substitute La^{3+} ions in only one crystallographic site of C_1 symmetry. The Pr concentration determined by inductively coupled plasma atomic spectroscopy is 0.2% which corresponds to $1.55\ 10^{19}$ at/cm^3.

The measurements were performed on the transition between the lowest crystal-field levels of the $^3H_4$ and $^1D_2$ multiplets at 602.76 nm (in vacuum) in $La_2(WO_4)_3$. The sample is a cube of $5\times5\times5$ mm^3. The sample was immersed in liquid helium at a temperature of 2.0 K.

A ring dye laser (Coherent 699–21) using Rhodamine 6G pumped by a $Nd:YVO_4$ laser (Coherent Verdi) provides 400 mW output power at $\lambda=602.76$ nm. The cw dye laser is linearly polarized and operates in a single servo-locked mode with a spectral width of 1 MHz. In order to create the desired pulse shapes and to eliminate beam movement accompanying frequency shifts, the laser light is passed twice through a 200 MHz acousto-optic modulator (AOM) with a bandwidth of 100 MHz. It is then sent through a 350 MHz AOM, which can be driven by two rf frequencies separated by a frequency equal to the splitting between two hyperfine levels of the $^3H_4(0)$ ground state. A 1 GS/s arbitrary waveform generator (Tektronix AWG520), that allows direct control of pulse amplitude, phase, and frequency, drives both AOMs.

After the 350 MHz AOM, the light passes through a single mode optical fiber to clean up the spatial mode. A beam splitter removes a small percentage of the light before the cryostat which is used as a reference beam. The rest of the beam goes through a $\lambda/2$ plate to adjust the light polarization to match the crystal orientation, and is then focused onto the $Pr^{3+}:La_2(WO_4)_3$ single crystal. The diameter of the focused beam is 100 μm. In order to only study ions in the center of the laser spot where the intensity varies less than 20%, the transmitted light is imaged onto a 50 μm pinhole before being focused on the detector.

The spectral structures, prepared by a hole-burning technique, are measured by scanning the light frequency and by recording the intensities of both the transmitted and the reference beams which are detected by Thorlabs PDB150A detectors. The probe pulse intensity was chosen such that the created spectral structures are unaffected by the readout process.

All the experiments performed in this study can be divided into three steps: (i) the preparation, (ii) the coherent manipulation, (iii) the read out. To coherently drive the optical transitions between the different hyperfine sublevels, we create a narrow peak of absorption consisting of an ensemble of selected identical ions on a background of zero absorption. The inhomogeneous absorption profile of the $^3H_4(0)\rightarrow{}^1D_2(0)$ transition has a linewidth of several GHz and the hyperfine splittings of Pr^{3+} ions are of the order of 10 MHz. To create a measurement situation similar to that of a narrow resonance line of a free atom or of an atom caught in trap, it is necessary to first prepare the optical inhomogeneous absorption profile so that the light only interacts with a selected group of ions absorbing on a specific transition.

The preparation step can also be divided into three steps. First, a wide spectral interval, called pit in the following, containing almost no absorbing ions, is cleared within the inhomogeneous absorption line. The possibility of creating such a pit is due to a hole-burning mechanism which, in the case of Pr^{3+} ions, comes from population redistributions between hyperfine sublevels in the $^3H_4(0)$ electronic ground state. Indeed, hyperfine ground-state lifetime is long compared with the lifetime of the excited state. In $Pr^{3+}:La_2(WO_4)_3$, the hyperfine ground-state lifetime is 16 s and the radiative lifetime of the $^1D_2(0)$ excited state is 61 μs.[18] Optical transitions can thus be cycled, i.e., the ions can be excited and allowed to relax, thousands of times before population relaxation between hyperfine levels becomes significant. Due to this large difference between the different lifetimes, it is possible to empty the population of two hyperfine ground-state levels within the pit and to put all the population in an third auxiliary storage hyperfine level. This method was introduced in Ref. 21 and applications can be found in Refs. 22 and 23. Second, we shift the laser frequency away from this pit to pump back ions absorbing within a narrow spectral interval into the emptied region. This procedure is henceforth called the burn-back pulse. Since the inhomogeneous broadening is large compared with the hyperfine splittings, the burn-back frequency will be resonant with all possible transitions within the hyperfine levels, but for different frequency classes of absorbers (nine in total as we will see in the following). Therefore, burning back at a single frequency brings back a complex pattern of transitions into the pit corresponding to different classes. Third, to be able to work only with a specific class of ions, some other pulses, henceforth called clean-wrong-class pulses, are applied to some transitions into the pit to get rid of the unwanted classes. We are then able to manipulate a specific optical transitions at a specific frequency without light interacting with other ions and other transitions. This preparation step allows us to determine the hyperfine ordering in the $^3H_4$ ground state and in the $^1D_2$ excited state and also the relative oscillator strengths between the individual hyperfine transitions.

After this preparation step, coherent manipulations of the system are performed to determine the absolute oscillator

strengths of the hyperfine transitions and the hyperfine inhomogeneous and homogeneous linewidths are obtained by free induction decay (FID) and Raman echo measurements.

Three different types of pulses were used in this work. The burn-back pulse is a complex hyperbolic secant pulse (sech pulse), commonly used in NMR (Ref. 24) for which the amplitude of the Rabi frequency, $\Omega(t)$, is given by

$$\Omega(t) = \Omega_{\max} \operatorname{sech}[\beta(t - t_0)], \tag{1}$$

where β (in rad/s) is related to the temporal width of the pulse by

$$t_{\mathrm{FWHM}} \approx \frac{1.76}{\beta} \tag{2}$$

t_{FWHM} is the full width half maximum of the intensity of the pulse. $\Omega_{\max}$ is the maximum Rabi frequency. The sech pulse has a tanh frequency chirp centered around the frequency ν_c,

$$\nu = \nu_c + \frac{\mu\beta}{2\pi}\tanh[\beta(t - t_0)], \tag{3}$$

where ν is the instantaneous frequency (Hz) and μ is a real constant. The frequency scan width of the pulse, f_{width}, which is the total span of the frequency sweep, is related to the pulse parameters β and μ by

$$f_{\mathrm{width}} = \frac{\mu\beta}{\pi}. \tag{4}$$

As demonstrated theoretically in Ref. 25 and experimentally in Refs. 23 and 26 sech pulse gives high-efficiency state-to-state population transfers which is important for efficiently bringing back ions with a specific hyperfine transition into the pit. In Ref. 26, de Seze *et al.* demonstrated population transfers close to 100% using sech pulse. In our work, the sech pulse has always the same characteristics with $t_{\mathrm{FWHM}}=1.6$ μs, $f_{\mathrm{width}}=1$ MHz and with a total truncated duration $t_{\mathrm{cutoff}}=8$ μs.

The pit cleaning procedure and the clean-wrong-class pulses are composed of several sechscan pulses which are a modification of a sech pulse. The center of the pulse is extended with a straight line in both amplitude and frequency. This type of pulse consists of the first half of a sech pulse of the form given by Eq. (1) with center frequency ν_1, a linear scan with constant amplitude, $\Omega_{\max}$, in the frequency range ν_1 to ν_2 and the second half of a sech pulse with amplitude $\Omega_{\max}$ and centered around the frequency ν_2. The sechscan pulse is used to clean larger frequency regions than is possible with the sech pulse.[23] For the pit creation, the sequence used in this work is composed of around 1200 sechscan pulses with $t_{\mathrm{FWHM}}=3$ μs, $t_{\mathrm{cutoff}}=86$ μs and with f_{width} depending on the frequency range to clean. Between each pulse, a waiting time of 1 ms is added to allow the population relaxation of the excited state.

Coherent driving of isolated hyperfine transitions are performed using super-Gaussian pulses. The amplitude of the Rabi frequency of such a pulse, $\Omega(t)$, is given by

$$\Omega(t) = \Omega_{\max} \exp\left[-\frac{1}{2}\left(\frac{t - t_0}{\sigma}\right)^{2m}\right], \tag{5}$$

with m is the order of the pulse, $m=3$ or 7 in this work. $m=1$ gives a Gaussian pulse. σ is related to the full width half maximum of the intensity t_{FWHM} by

$$\sigma = \frac{t_{\mathrm{FWHM}}}{2\sqrt{\ln 2}}. \tag{6}$$

Compared to a Gaussian pulse, the super-Gaussian pulse has a flatter top. For coherent driving, short super-Gaussian pulses spectrally flat across the prepared peak were used in order to reduce inhomogeneities of Rabi frequencies. Short Gaussian pulses could have been used, however, the pulses also have to be spectrally selective which means that no spectator ions, i.e., ions outside the pit, are affected by the pulse. The super-Gaussian pulse is a good compromise between spectral selectivity and low Rabi frequency inhomogeneity. In the present work, the temporal characteristics of these pulses are typically $t_{\mathrm{FWHM}}=1$ μs, $t_{\mathrm{cutoff}}=3$ μs.

III. HYPERFINE ORDERING AND RELATIVE OSCILLATOR STRENGTHS BETWEEN INDIVIDUAL HYPERFINE TRANSITIONS

A. Hyperfine ordering

Pr has one 100% abundant isotope (^{141}Pr) with a nuclear spin $I=5/2$. In a C_1 low site symmetry, the electronic degeneracy of the $^3H_4$ and $^1D_2$ multiplets is totally lifted giving rise to electronic singlets. In a particular hyperfine manifold, at zero magnetic field, the following effective spin Hamiltonian can be used to describe the hyperfine splittings:[27]

$$H = \mathbf{I} \cdot (A_J^2 \mathbf{\Lambda} + \mathbf{P}) \cdot \mathbf{I} \tag{7}$$

where $\mathbf{I}$ is the nuclear spin, $\mathbf{P}$ the pure quadrupole tensor, and the $\mathbf{\Lambda}$ tensor is given by

$$\Lambda_{\alpha\beta} = \sum_{n=1}^{2J+1} \frac{\langle 0|J_\alpha|n\rangle\langle n|J_\beta|0\rangle}{E_n - E_0}. \tag{8}$$

The index 0 denotes the first crystal-field singlet level of the $^3H_4$ and $^1D_2$ multiplets, n the other crystal-field levels, E_n is the energy of the crystal-field level. α and β stands for x, y, z. A_J is the hyperfine constant of the J multiplet. At zero magnetic field, the hyperfine splittings are due to a "pseudoquadrupole interaction" which is the combination of the second-order hyperfine interaction and of the pure nuclear quadrupole interaction [Eq. (7)]. In low site symmetry, the principal axes of the $\mathbf{P}$ and $\mathbf{\Lambda}$ tensors are not coincident. However, we can define a third set of principal axes (x',y',z') which gives the following form for the effective Hamiltonian:[28]

$$H' = D[I_{z'}^2 - I(I+1)/3] + E(I_{x'}^2 - I_{y'}^2). \tag{9}$$

Each crystal-field level of a J multiplet is characterized by a set of D and E values and by its own principal axes.[29] This Hamiltonian splits the $^3H_4(0)$ and $^1D_2(0)$ into three doubly degenerate hyperfine levels.

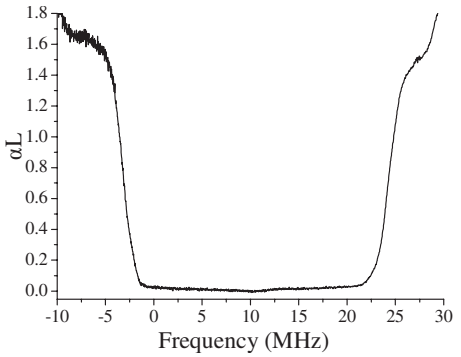

FIG. 1. Spectral hole-burning in the inhomogeneously broadened $^3H_4(0) \rightarrow {}^1D_2(0)$ transition in 0.2% $Pr^{3+}:La_2(WO_4)_3$. At 2.0 K, a 22.5 MHz wide spectral interval (a pit) was completely emptied of absorbing ions. αL is the optical depth where α is the absorption coefficient and L the length of the crystal. The amount of Pr^{3+} ions absorbing at a particular frequency is monitored by recording the absorption.

We have already obtained in the frequency domain the hyperfine structure of the $^3H_4(0)$ ground state and of the $^1D_2(0)$ excited state by conventional spectral hole burning.[18] However, as the spectral positions of side holes and antiholes are symmetric around the central hole, such a study did not allow us to determine the ordering of the hyperfine levels for both states, the signs of D and E could not be specified. Moreover, the relative oscillator strengths between each individual hyperfine transitions could not be obtained without assumptions about relative oscillator strengths and about relaxation rates between the ground state hyperfine levels. In the following δ_1^g, δ_2^g, δ_1^e, and δ_2^e are the hyperfine splittings of the $^3H_4(0)$ ground state and of the $^1D_2(0)$ excited state, respectively. By applying the sequence described in Sec. II which consists of cleaning a pit in the inhomogeneous broaden $^3H_4(0) \rightarrow {}^1D_2(0)$ transition and then bringing back ions at a specific hyperfine transitions into this pit by applying a burn-back pulse, the ordering of the hyperfine levels is determined, as well as the relative oscillator strengths between the three transitions starting from the selected ground-state hyperfine level to the three excited hyperfine levels.

In the case of $Pr^{3+}:La_2(WO_4)_3$, a maximum pit of around 22.5 MHz was created into the absorption band (Fig. 1). The amount of Pr^{3+} ions absorbing at a particular frequency was monitored by recording the absorption. At frequencies inside the hole, the signal is quasiconstant and is less than 0.5% of the absorption signal before burning (Fig. 1).

To simplify the discussion and the analysis of the data, we assume that the ordering of the hyperfine splittings as well as the label of these levels is the same in $Pr^{3+}:La_2(WO_4)_3$ as in $Pr^{3+}:Y_2SiO_5$.[22] This assumption will be experimentally checked. The energy level diagram of Pr^{3+} ions is shown on the left hand side of Fig. 2(a). We assume that $\delta_1^g = 24.6$ MHz, $\delta_2^g = 14.9$ MHz, $\delta_1^e = 5.0$ MHz, and $\delta_2^e = 7.3$ MHz. These splittings are from Ref. 18. To simplify the notation in Fig. 2(a), for example, $5/2g$ stands for the ground state wave function $|M_I = \pm \frac{5}{2}\rangle$ where M_I is the nuclear spin projection. It is important to notice that due to the low site symmetry of Pr^{3+} ions in $La_2(WO_4)_3$ the nuclear

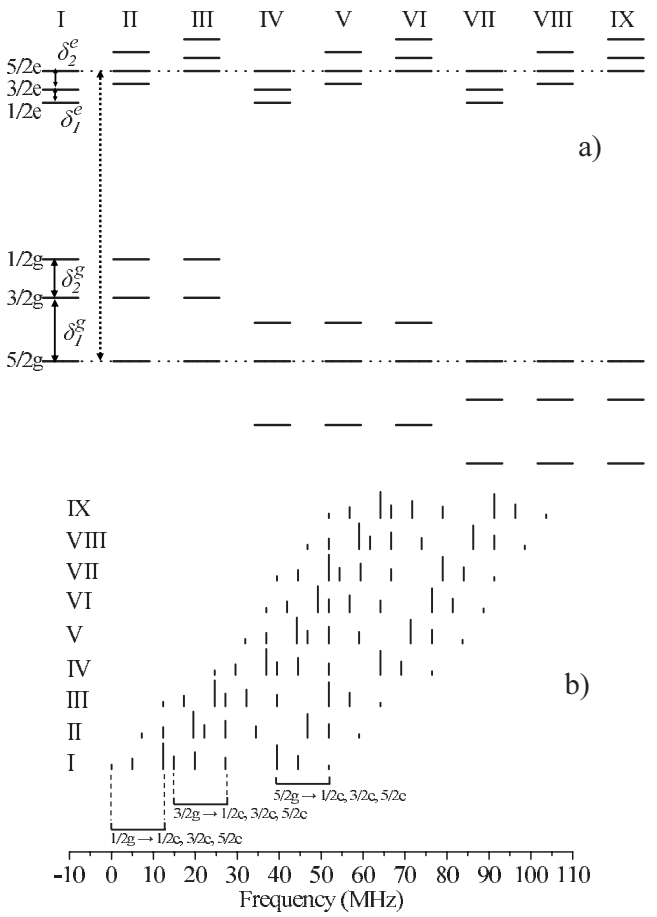

FIG. 2. (a) Hyperfine energy level diagram of the $^3H_4(0) \rightarrow {}^1D_2(0)$ transition of Pr^{3+} in $La_2(WO_4)_3$. δ_1^g, δ_2^g, δ_1^e, and δ_2^e are the hyperfine splittings of the $^3H_4(0)$ ground state and of the $^1D_2(0)$ excited state, respectively. For the eigenstates, $5/2g$ corresponds, for example, to the $|M_I = \pm \frac{5}{2}\rangle$ wave function of the ground state. The burn-back frequency (dashed arrow) is on the $5/2g \rightarrow 5/2e$ transition for class I. Due to the inhomogeneous distribution of optical resonance frequencies, different absorbers (nine classes in total, I–IX) have different transitions resonant with the burning field. (b) Stick diagram showing all the frequency positions of the different hyperfine transitions for all the different classes I–IX. The lengths reproduce the relative oscillator strengths calculated in this section.

wave functions are mixed and M_I is not strictly a good quantum number. In the following, the zero of frequencies is chosen into the pit at the position shown in Fig. 1.

The burn-back pulse is at a frequency $\delta_1^g + \delta_2^g + \delta_1^e + \delta_2^e = 51.8$ MHz away from this zero with $t_{FWHM} = 1.6$ μs, $f_{width} = 1$ MHz and $t_{cutoff} = 8$ μs. Due to the inhomogeneous broadening, each allowed transition between the hyperfine levels of the ground and the excited states is resonant with the frequency of the burning laser for some subset of ions. It means that this frequency can correspond to the $5/2g \rightarrow 5/2e$ transition for one class of ions [class I of Fig. 2(a)], to the $5/2g \rightarrow 3/2e$ transition for another class of ions [class II of Fig. 2(a)] etc. All in all, nine different classes of Pr^{3+} ions can be excited [classes I–IX in Fig. 2(a)]. For our arbitrary choice, the zero of frequency corresponds to the $1/2g \rightarrow 1/2e$ transition of class I.

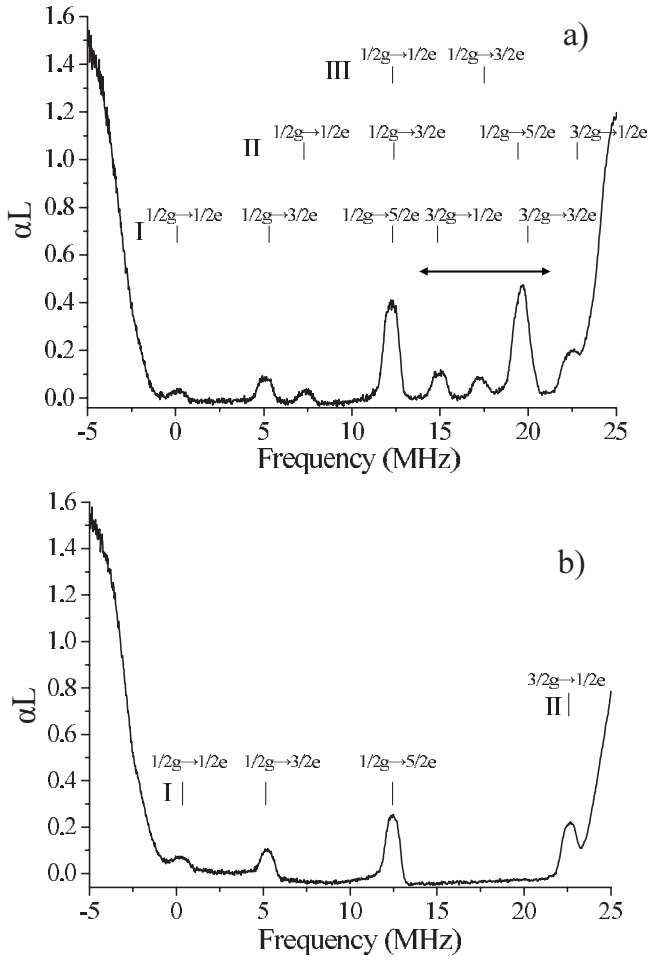

FIG. 3. Ions absorbing within a pit in the inhomogeneously broaden $^3H_4(0) \rightarrow {}^1D_2(0)$ transition in 0.2% Pr^{3+}:$La_2(WO_4)_3$. (a) A 22.5 MHz interval was completely emptied of absorbing ions through spectral hole burning. Then different classes of Pr^{3+} ions have been pumped back into the pit by shifting the laser frequency by 51.8 MHz to excite ions from an auxiliary ground-state hyperfine level and let them relax into a new hyperfine level. All the observed transitions are attributed to a particular hyperfine transition belonging to the three different classes I–III. (b) Starting from (a), clean-wrong-class pulses are applied in the 14–21 MHz range [see arrow in (a)] to empty the $1/2g$ level of class II and III. The three transitions of class I starting from level $1/2g$ are isolated. The relative oscillator strengths can be calculated by integration of the line intensities.

A stick diagram of all the different hyperfine transitions which can be obtained for all the different classes is shown in Fig. 2(b). Due to our assumption on the ordering of the hyperfine splittings, for each class, the hyperfine transitions are always in the following order: $1/2g \rightarrow 1/2e$, $3/2e$, $5/2e$ then $3/2g \rightarrow 1/2e$, $3/2e$, $5/2e$ and $5/2g \rightarrow 1/2e$, $3/2e$, $5/2e$. The stick lengths reproduce the relative oscillator strengths determined in this section [Fig. 2(b)].

As the pit is in the 0–23 MHz range, only the hyperfine transitions falling in this frequency range are seen by scanning the hole after the burn-back pulse. Figure 3(a) shows the result of an experiment where a pit is first created, then one burn-back pulse at 51.8 MHz is applied. The burn-back pulse brings back some transitions into the pit which can be analyzed by the stick diagram of Fig. 2(b). All the transitions can be attributed to three different classes (I, II, and III) of Pr^{3+} ions [Fig. 3(a)]. The ordering of the splittings in the excited state as well as in the ground state can be obtained from, e.g., hyperfine transitions corresponding to class I. The two transitions $1/2g \rightarrow 1/2e$ and $1/2g \rightarrow 3/2e$ of class I separated by 5 MHz and the two transitions $1/2g \rightarrow 3/2e$ and $1/2g \rightarrow 5/2e$ of class I separated by 7 MHz confirm that in the $^1D_2(0)$ excited state the hyperfine splitting are in the order which was assumed in Fig. 2(a). The transitions $1/2g \rightarrow 1/2e$ and $3/2g \rightarrow 1/2e$ of class I separated by 14.9 MHz confirm also our hypothesis for the ground state.

From the ordering of the hyperfine splittings and by using Eq. (9), the sign of the D parameter can be retrieved. However, the sign of the E parameter cannot be obtained because the matrix corresponding to (D,E) or $(D,-E)$ in the $\{|M_I\rangle\}$ basis set have the same eigenvalues. These matrices also have the same eigenvectors so that the mixing is finally independent on the sign of E but rather depend on the ratio $\frac{E}{D}$.[30] $D=-6.35\pm0.05$ MHz, $E=\pm0.88\pm0.05$ MHz, and $D=+1.92\pm0.05$ MHz, $E=\pm0.36\pm0.05$ MHz for the $^3H_4(0)$ ground state and the $^1D_2(0)$ excited state, respectively.

B. Relative oscillator strengths between the individual hyperfine transitions

To determine the relative oscillator strengths between the different hyperfine transitions, we isolated (i) only one class of ions (class I was chosen) and (ii) three transitions starting from the same hyperfine ground state level to the three excited hyperfine levels. Three different hole-burning sequences were used to measure the relative intensities of the transitions starting from $1/2g$, $3/2g$, and $5/2g$.

1. Relative oscillator strengths starting from 1/2g

To measure the relative oscillator strengths between the three hyperfine transitions $1/2g \rightarrow 1/2e$, $1/2g \rightarrow 3/2e$ and $1/2g \rightarrow 5/2e$ for class I, a pit is first cleaned in the 0–25 MHz range, then a burn-back pulse at 51.8 MHz is applied. As we can see from Fig. 3(a), these three transitions are brought back into the pit. However, some of the transitions of class II and class III are at the same frequency as some transitions of class I. This is the case for example of transitions $1/2g \rightarrow 3/2e$ of class II and $1/2g \rightarrow 1/2e$ of class III at 12.4 MHz which are at the same frequency of transition $1/2g \rightarrow 5/2e$ of class I [Fig. 3(a)]. To perform a reliable measurement of the relative oscillator strengths between the hyperfine transitions starting from level $1/2g$, the contributions of class II and III have to be cancelled. This is performed by applying 30 clean-wrong-class pulses in the 14–21 MHz range [see the arrow in Fig. 3(a)] with a 1 ms delay between each pulse. The 30 sechscan pulses are characterized by $t_{FWHM}=2$ μs with a total truncated duration $t_{cutoff}=20$ μs. Levels $1/2g$ of class II and $1/2g$ of class III will be emptied by cleaning the transitions $1/2g \rightarrow 5/2e$ of class II at 19.6 MHz and $1/2g \rightarrow 3/2e$ of class III at 17.3 MHz. The result is shown on Fig. 3(b) where only transitions $1/2g \rightarrow 1/2e$, $1/2g \rightarrow 3/2e$, and $1/2g \rightarrow 5/2e$ of class I re-

TABLE I. Relative oscillator strengths for transitions between the $^3H_4(0)$ and $^1D_2(0)$ hyperfine manifolds in Pr^{3+}:$La_2(WO_4)_3$ as calculated from absorption data. Rows correspond to transitions starting from the ground state hyperfine levels. Columns correspond to transitions to different excited state hyperfine levels.

	$1/2e$	$3/2e$	$5/2e$
$1/2g$	0.09 ± 0.01	0.28 ± 0.01	0.63 ± 0.01
$3/2g$	0.33 ± 0.01	0.39 ± 0.01	0.28 ± 0.02
$5/2g$	0.55 ± 0.01	0.36 ± 0.01	0.09 ± 0.01

main in the 0–15 MHz range. By integrating each of the three transitions and constraining the sum to one, we obtain the first row of Table I. The uncertainty is obtained by repeating the same experiment several times.

2. Relative oscillator strengths starting from **3/2g**

To determine the relative oscillator strengths between the three hyperfine transitions $3/2g \rightarrow 1/2e$, $3/2g \rightarrow 3/2e$, and $3/2g \rightarrow 5/2e$ for class I, the pit has to be centered in the 10–30 MHz frequency range where these transitions are lying [Fig. 2(b)]. This shift is obtained by cleaning the same pit as in the previous experiment and then by burning back the transitions at 41.8 MHz. This burn-back pulse which is always on the $5/2g \rightarrow 5/2e$ transition for class I is equivalent to a positive 10 MHz shift of the pit [Fig. 4(a)]. It is more difficult in this case to isolate transitions of class I. Indeed, as can be seen from Fig. 4(a) and compared with the previous case where only one hyperfine transition of this class had contributions of other type of classes, two hyperfine transitions of class I have some contributions of class II and class III: the transition $3/2g \rightarrow 3/2e$ of class I has a contribution of the transition $1/2g \rightarrow 5/2e$ of class II; the transition $3/2g \rightarrow 5/2e$ of class I has a contribution of the transition $3/2g \rightarrow 3/2e$ of class II and of the transition $3/2g \rightarrow 1/2e$ of class III. We get rid of the contribution of class III by emptying the population of the $3/2g$ state. However, in the case of class II, the two hyperfine $1/2g$ and $3/2g$ ground-state levels have to be simultaneously emptied.

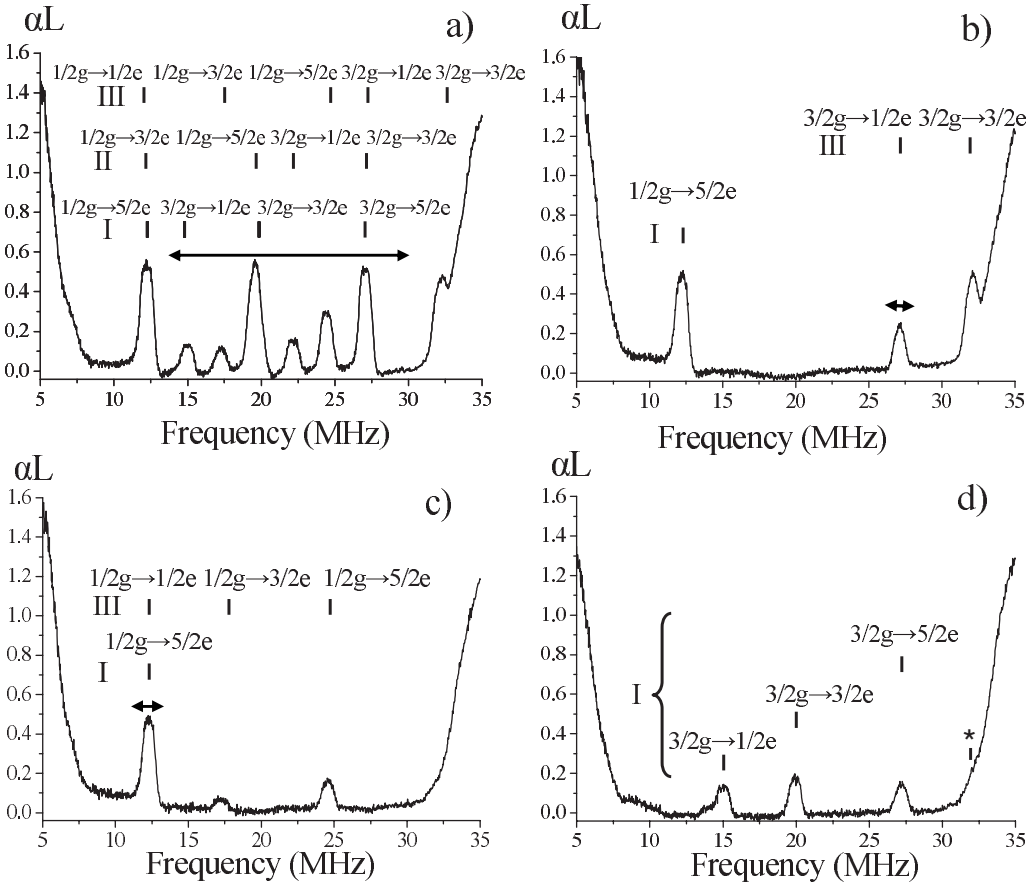

FIG. 4. Ions absorbing within a pit in the inhomogeneous broadened $^3H_4(0) \rightarrow {}^1D_2(0)$ transition in 0.2% Pr^{3+}:$La_2(WO_4)_3$. (a) Different classes of Pr^{3+} ions were pumped back into the pit, by shifting the laser frequency by 41.8 MHz. All the observed transitions are attributed to a particular hyperfine transition of the three different classes I to III. (b) Starting from (a) clean-wrong-class pulses were applied in the 14–30 MHz range [see arrow in (a)] to empty the level $3/2g$ of the class I and levels $1/2g$ and $3/2g$ of classes II and III. Some population remains on the level $3/2g$ of class III. (c) Starting from (b), clean-wrong-class pulses centered on the transition $3/2g \rightarrow 1/2e$ of class III at 27 MHz were applied to empty the starting level [see arrow in (b)]. All the population of level $3/2g$ of class III is transfered to levels $1/2g$ and $5/2g$. (d) Starting from (c), clean-wrong-class pulses centered at 12.3 MHz [see arrow in (c)] are applied to transfer for the class I population from level $1/2g$ to levels $3/2g$ and $5/2g$. The main contribution is now due to the class I. A small contribution of class III indicated by a star can be seen on the wall of the pit.

We first applied 30 clean-wrong-class pulses in the 14–30 MHz range with $t_{FWHM}=2$ μs, $t_{cutoff}=20$ μs, and with 1 ms delay between each pulse. This procedure aims at emptying levels $3/2g$ for class I and levels $1/2g$ and $3/2g$ for classes II and III. The result is shown in Fig. 4(b). All the population of class I is transferred to states $1/2g$ and $5/2g$ (transitions starting from $5/2g$ are outside the hole). For class II, we managed to empty levels $1/2g$ and $3/2g$. However, some population remains in the $3/2g$ state of class III as can be seen from Fig. 4(b). 16 clean-wrong-class pulses centered on the transition $3/2g \rightarrow 1/2e$ at 27 MHz with $t_{FWHM}=3$ μs, $t_{cutoff}=40$ μs, $f_{width}=0.5$ MHz and with 1ms delay between each pulse were applied to empty this level. The result is shown on Fig. 4(c) where all the population of the level $3/2g$ of class III was transferred to level $1/2g$ and $5/2g$. At this step of the procedure, in the pit, there remains only transitions starting from level $1/2g$ for classes I and III. By comparing the intensity of the $1/2g \rightarrow 5/2e$ transition of class III between Figs. 4(a) and 4(c), the contribution of this class to the spectrum has decreased. Finally, we transferred class I and class III population from level $1/2g$ to levels $3/2g$ and $5/2g$ by applying clean-wrong-class pulses centered at 12.3 MHz with $t_{FWHM}=3$ μs, $t_{cutoff}=40$ μs, and $f_{width}=0.5$ MHz. At the end of this burning sequence [Fig. 4(d)], only class I with population in the $3/2g$ remains in the pit and actually very little population was transferred to level $3/2g$ of class III. Indeed a small bump corresponding to the $3/2g \rightarrow 3/2e$ transition of class III [indicated by a star in Fig. 4(d)] can be seen in the wall of the pit. The population in the $3/2g$ of class III is very small if we compare the intensity of the $3/2g \rightarrow 3/2e$ transition between Figs. 4(b) and 4(d). The line at 27.2 MHz is mainly composed of the $3/2g \rightarrow 5/2e$ transition of class I with a small contribution of the $3/2g \rightarrow 1/2e$ transition of class III. As it was not possible to completely empty level $3/2g$ of class III, in the second row of Table I, this small contribution is taken into account by a larger uncertainty on the relative oscillator strength for the $3/2g \rightarrow 5/2e$ transition.

Another contribution is seen on the left hand side of transition $3/2g \rightarrow 1/2e$ [Fig. 4(d)], the origin of this is not known. To calculate the relative oscillator strengths, a deconvolution procedure is used to get rid of this contribution.

3. Relative oscillator strengths starting from **5/2g**

To measure the relative oscillator strengths between the three hyperfine transitions $5/2g \rightarrow 1/2e$, $5/2g \rightarrow 3/2e$, and $5/2g \rightarrow 5/2e$, the burn-back pulse is now chosen on the $1/2g \rightarrow 1/2e$ transitions. Figures 5(a) and 5(b) gather the nine different excited classes as well as the different transitions corresponding to these classes. To centered the pit on the 32–55 MHz range where all the three hyperfine transitions $5/2g \rightarrow 1/2e$, $5/2g \rightarrow 3/2e$, and $5/2g \rightarrow 5/2e$ of class I are falling [see Fig. 5(b)], the burn-back pulse is put at −32.2 MHz. By using the stick diagram of Fig. 5(b), the lines which appear in the 32–55 MHz range [Fig. 6(a)] are attributed to transitions of class I, II, and III. The contribution of class II can be eliminated by applying clean-wrong-class pulses in the 33–36 MHz range. Figure 6(b) shows that this contribution has indeed disappeared. We cannot remove

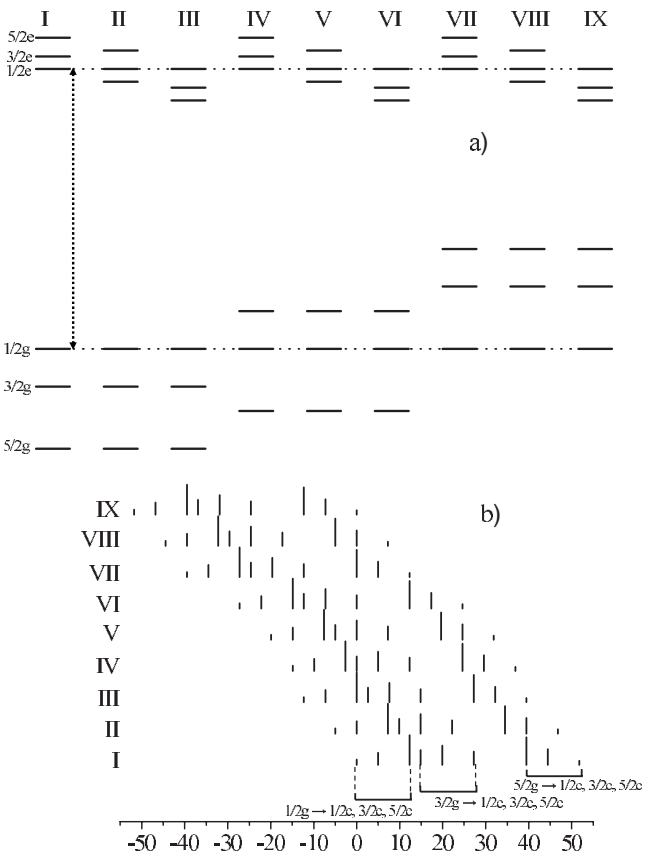

FIG. 5. (a) Hyperfine energy level diagram of the $^3H_4(0) \rightarrow {}^1D_2(0)$ transition of Pr^{3+} in $La_2(WO_4)_3$. The burn-back frequency (dashed arrow) is on the $1/2g \rightarrow 1/2e$ transition for class I. (b) Stick diagram of all the different hyperfine transitions which can be obtained for all the different classes.

the contribution of the transition $5/2g \rightarrow 5/2e$ of class III to the transition $5/2g \rightarrow 1/2e$ of class I at 39.4 MHz. However as the transition $5/2g \rightarrow 5/2e$ is very weak compared to the transition $5/2g \rightarrow 1/2e$ (see the transition $5/2g \rightarrow 5/2e$ of class I at 51.7 MHz), this brings a small contribution which lies in the uncertainty of the measurements. From Fig. 6(b), the relative oscillator strengths of the hyperfine transitions starting from the $5/2g$ level is calculated and given in the third row of Table I.

From Table I, although there is no direct connection between the measured absorption from different ground state hyperfine levels, the sum of the relative strengths of transitions going from each excited state to all ground state levels is found to be approximately one. This indicates that the relative oscillator strengths estimation is reliable.

IV. ABSOLUTE OSCILLATOR STRENGTHS DETERMINATION BY RABI FLOPPING

The absolute oscillator strengths were obtained by studying Rabi flopping through coherent driving of the transitions. We first prepared a spectrally isolated peak due to ions absorbing on a specific transition. We used the same preparation sequence as for Fig. 3(b) and we focused on the $1/2g \rightarrow 5/2e$ transition of class I. A coherent super-Gaussian pulse

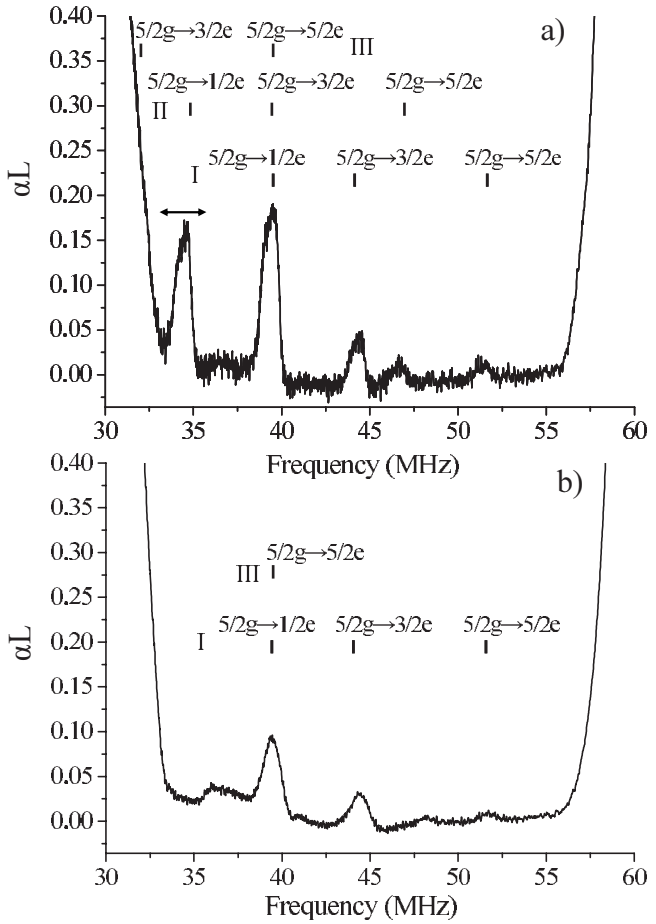

FIG. 6. Ions absorbing within a pit in the inhomogeneous broadened $^3H_4(0) \rightarrow {}^1D_2(0)$ transition in 0.2% $Pr^{3+}:La_2(WO_4)_3$. (a) After cleaning a 22.5 MHz interval, different classes of Pr^{3+} ions were pumped back into the pit, by shifting the laser frequency by −32.2 MHz. All the observed transitions are attributed to particular hyperfine transitions belonging to three different classes I to III. (b) Starting from (a) clean-wrong-class pulses are applied in the 33–36 MHz range [see arrow in (a)] to empty the $5/2g$ level of class II. The three transitions of class I starting from level $5/2g$ are isolated with a small contribution of the transition $5/2g \rightarrow 5/2e$ of class III at 39.4 MHz.

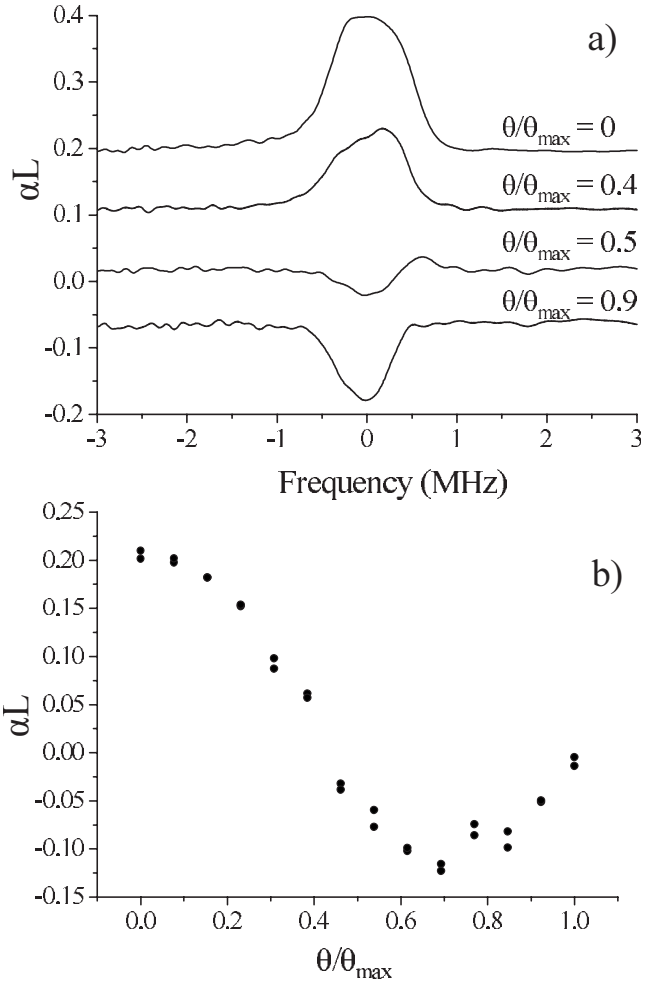

FIG. 7. (a) Transmission of the $1/2g \rightarrow 5/2e$ transition for different values of the pulse area. For the sake of clarity, the spectra are vertically shifted. (b) Coherent driving of the $1/2g \rightarrow 5/2e$ transition. Super-Gaussian pulses with $t_{FWHM}=0.5$ μs, $t_{cutoff}=1.5$ μs and with variable pulse area ($\theta=\Omega t$) were applied to the transition. θ_{max} is 1.3π in our experiment. The population difference between the ground and the excited state is obtained by recording the transmission across the transition 8 μs after the coherent pulse.

of order 3 with $t_{FWHM}=0.5$ μs, $t_{cutoff}=1.5$ μs and with a variable pulse area $\theta(\theta=\Omega t)$ was applied to this transition. We used such short super-Gaussian pulses spectrally flat across the $1/2g \rightarrow 5/2e$ transition in order to reduce the inhomogeneities of Rabi frequencies linked to ions absorbing at slightly different frequencies. The population difference between the $1/2g$ and $5/2e$ states was monitored 8 μs after the super-Gaussian pulse by recording the transmission at the resonance frequency through a 50 μm diameter pinhole.

The pulse area θ is the angle through which the state vector was rotated in the Bloch sphere. When θ is increased the ions are driven up into the excited state and the absorption decreases [Fig. 7(a)]. When Pr^{3+} ions are driven more than halfway up into the excited state ($\theta > \frac{\pi}{2}$), a majority of the population is in this state and stimulated emission can be observed [see Fig. 7(a) for $\frac{\theta}{\theta_{max}}=0.5, 0.9$]. For Figs. 7(a) and 7(b), $\theta_{max}=1.3\pi$ is the maximum pulse area obtained in our experiment limited by the input laser power. The value of the pulse area refers to the transition $1/2g \rightarrow 5/2e$ of site I in $Pr:Y_2SiO_5$. The setup is calibrated using the Rabi frequencies and oscillator strengths of Pr^{3+} in the silicate host.[22]

This absorption-emission balance shows oscillation as a function of the applied pulse area from which the absolute oscillator strength of the $1/2g \rightarrow 5/2e$ transition can be determined [Fig. 7(b)]. A decay of the Rabi frequency oscillation indicates that inhomogeneities in the Rabi frequency still remain. This could be due to the fact that ions at different spatial positions in the laser beam have different Rabi frequencies due to a variation in field intensity across the beam. This variation was limited by the use of a 50 μm diameter pinhole on the detection side which imaged only the center of the beam. From the Rabi flopping, it can be seen that a π pulse in $Pr:La_2(WO_4)_3$ is obtained for $\frac{\theta}{\theta_{max}}=0.69$ [Fig. 7(b)]. As $\theta_{max}=1.3\pi$, it is equivalent to a pulse area of 0.897π for $Pr:Y_2SiO_5$. The transition dipole moment

for the $1/2g \rightarrow 5/2e$ transition in $Pr:Y_2SiO_5$, $\mu_{1/2g\rightarrow 5/2e}^{Y_2SiO_5}$, is: $\mu_{1/2g\rightarrow 5/2e}^{Y_2SiO_5} = \sqrt{\frac{0.07}{0.93}}\mu_{5/2g\rightarrow 5/2e}^{Y_2SiO_5} = \sqrt{\frac{0.07}{0.93}} \times 2.6 \times 10^{-33} = 7.14 \times 10^{-33}$ C m. The ratio $\frac{0.07}{0.93}$ is taken from the relative oscillator strengths calculated in Ref. 22 for Y_2SiO_5, and the value of $\mu_{5/2g\rightarrow 5/2e}^{Y_2SiO_5}$ is coming from the erratum of Ref. 22. This implies that dipole moment for the $1/2g \rightarrow 5/2e$ transition in $Pr:La_2(WO_4)_3$, $\mu_{1/2g\rightarrow 5/2e}^{La_2(WO_4)_3}$, is $\frac{7.14\times 10^{-33}}{0.897} = 7.96 \times 10^{-33}$ Cm. From this calculation, we deduce that the oscillator strength of the $1/2g \rightarrow 5/2e$ transition in $Pr:La_2(WO_4)_3$, $f_{1/2g\rightarrow 5/2e}^{La_2(WO_4)_3}$, is 4.4×10^{-8}. The oscillator strength of the $5/2g \rightarrow 5/2e$ transition in Y_2SiO_5 ($f_{5/2g\rightarrow 5/2e}^{Y_2SiO_5} = 4.7 \times 10^{-7}$ from Ref. 22) is 10.7 times higher than the strongest transition in $La_2(WO_4)_3$. By considering the ratio gathered in Table I, the absolute oscillator strengths of all the other hyperfine transitions can be obtained.

V. INHOMOGENEOUS AND HOMOGENEOUS HYPERFINE LINEWIDTHS

To completely analyze the Λ system, the inhomogeneous and homogeneous hyperfine linewidths of the ground-state hyperfine levels, also called inhomogeneous and homogeneous Raman linewidth, have to be measured. The inhomogeneous broadening was measured by free induction decay. The energy level diagram used for this measurement is shown on Fig. 8(a). This linewidth is obtained by optically exciting a hyperfine coherence between the two $1/2g$ and $3/2g$ ground-state levels. The first step is meant to initiate a peak of class I ions in their $1/2g$ state. A bichromatic laser pulse at the two frequencies ω_1 and ω_2 is then tuned on the $1/2g \rightarrow 5/2e$ and $3/2g \rightarrow 5/2e$ transitions, respectively, and sent onto the system [see Figs. 8(a) and 8(b)]. The two pulses are super-Gaussian pulses with $m=3$, $t_{FWHM}=1$ μs, $t_{cutoff}=3$ μs. These two frequencies are separated by $\delta_2^g = 14.9$ MHz which is the hyperfine splitting between levels $1/2g$ and $3/2g$. A hyperfine coherence is created between these two levels which means that the state of the atoms acquires a component in the equatorial plane of the Bloch sphere corresponding to an oscillating dipole moment which radiates. Maximum dipole moment emission comes from atoms that experience a pulse area equal to $\frac{\pi}{2}$. Since the transitions are inhomogeneously broadened, the atoms oscillate at different frequencies, they then start to dephase and the decrease in rate of emission is the FID. As the dephasing is faster if atoms have large frequency spread, the FID gives information on the inhomogeneous hyperfine linewidth. The decay time of the hyperfine FID is noted $T_{2,Raman}^*$ and is related to the inhomogeneous linewidth by $T_{2,Raman}^* = \frac{1}{\pi\Gamma_{Raman}^*}$. As we excite the hyperfine coherence by means of two optical pulses at ω_1 and ω_2, optical coherences are also excited on the $1/2g \rightarrow 5/2e$ and $3/2g \rightarrow 5/2e$ transitions and optical FID also occurs on these two transitions. To obtain a reliable hyperfine FID measurement, we have to get rid of the optical FIDs during the read out. This is obtained by transferring the hyperfine FID on an optical transition which has not been optically excited by the bichromatic pulse. By applying a super-Gaussian read-out pulse at the frequency ω_3 on the $1/2g \rightarrow 3/2e$ transition [Figs. 8(a) and 8(b)], part of the hyperfine coherence will be transferred to the $3/2g \rightarrow 3/2e$ transition at ω_4. The dipole moment at this frequency starts to radiate and the decrease in the rate of emission as a function of T exactly follows the hyperfine FID. The emission at ω_4 beats with the detection pulse at a beatnote equal to δ_2^g. The FID is observed by measuring the amplitude of the beatnote by Fourier transform of the signal. By increasing the delay T between the bichromatic pulse and the read-out pulse, the amplitude of the beating decays with T as $e^{-T/T_{2,Raman}^*}$.

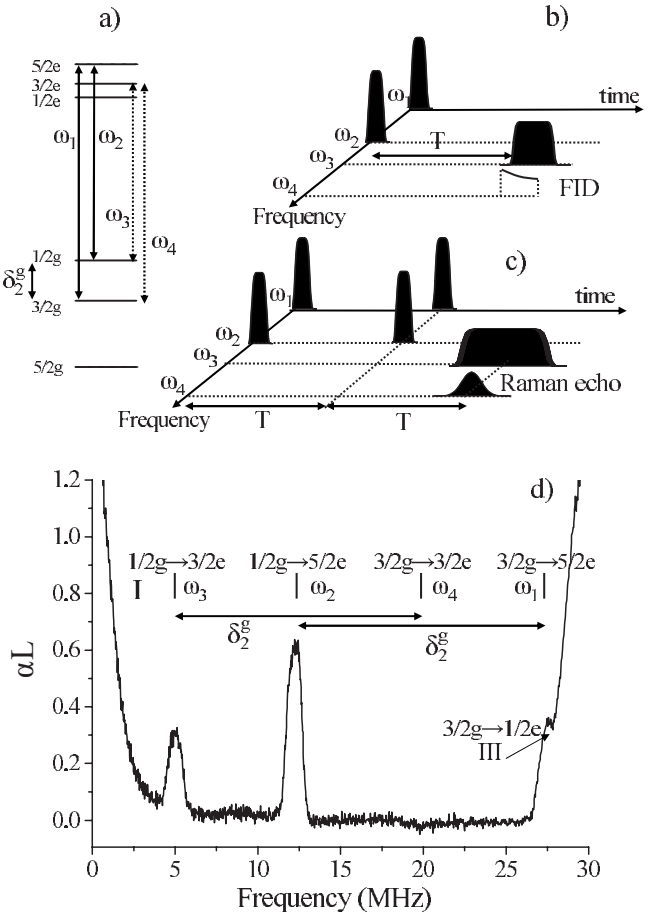

FIG. 8. a) Energy level diagram of Pr^{3+} for the $^3H_4(0) \rightarrow {}^1D_2(0)$ transition in $La_2(WO_4)_3$. The hyperfine coherences are excited by a bichromatic pulse at the two frequencies ω_1 and ω_2 tuned on the $1/2g \rightarrow 5/2e$ and $3/2g \rightarrow 5/2e$ transitions. The read-out depicted by dashed arrows is performed by applying a super-Gaussion pulse at the frequency ω_3 on the $1/2g \rightarrow 3/2e$ transition which transfers the hyperfine coherence on the transition $3/2g \rightarrow 3/2e$ at ω_4. [(b) and (c)] FID and Raman echo sequences, respectively. The probing is performed on the $1/2g \rightarrow 5/2e$ optical transition which has not been excited by the first bichromatic pulse. T is the delay between the first pulse and the probing for the FID experiment and between the first and the second bichromatic pulse for the Raman echo. The FID and the Raman echo are observed by measuring the amplitude of the beatnote between ω_3 and ω_4 by means of Fourier transform. (d) Preparation step before the FID and echo sequences. Only class I appears with a small contribution of class III. The different frequencies are indicated on the graph as well as the hyperfine splitting δ_2^g.

To measure the homogeneous linewidth of the ground state hyperfine levels, an additional bichromatic pulse is applied after a delay T and at the same frequencies ω_1 and ω_2 [Figs. 8(c)]. The effect of this second pulse is to reverse the Raman coherence evolution, and at a time T after the second pulse all atoms again oscillate with the same phase which gives rise to a Raman echo [Fig. 8(c)]. The read out is performed in the same way as for the FID with a super-Gaussian pulse at the frequency ω_3 ($m=7$, $t_{\mathrm{FWHM}}=4$ μs, $t_{\mathrm{cutoff}}=12$ μs) centered on the maximum Raman echo intensity [Fig. 8(c)]. The Raman echo is converted into an optical echo at frequency ω_4 and we then get rid of the contribution of the two optical echoes which appear on transitions $1/2g \rightarrow 5/2e$ and $3/2g \rightarrow 5/2e$. The Raman echo decays with T as $e^{-2T/T_{2,\mathrm{Raman}}}$ where $T_{2,\mathrm{Raman}}$ is the hyperfine coherence lifetime.

Before observing these two coherent transients, the system has to be prepared in such a way that only one class of ions undergoes these coherent manipulations. This requires that all the four transitions $\omega_1-\omega_4$ fall into the pit. As $\omega_1=27.2$ MHz, $\omega_2=12.3$ MHz, $\omega_3=5.0$ MHz, and $\omega_4=19.9$ MHz, the maximum difference between these four frequencies is $\omega_1-\omega_3=22.2$ MHz. As the maximum width of the pit obtained in this work is 22.5 MHz, all these transitions can in principle fall into the pit. The preparation step is the following: a pit of 22.5 MHz was cleaned, then a burnback pulse at 48.8 MHz with $t_{\mathrm{FWHM}}=1.7$ μs, $t_{\mathrm{cutoff}}=8$ μs, was applied. Clean-wrong class pulses with $t_{\mathrm{FWHM}}=2$ μs, $t_{\mathrm{cutoff}}=20$ μs, were applied in the 12–27 MHz range. The results are shown on Fig. 8(d). All the transitions with the frequencies ω_1 to ω_4 are within the pit. Apart from a small contribution of class III, only class I ions were selected [Fig. 8(d)]. The different frequencies are indicated on the graph as well as the hyperfine splitting δ_2^g between ω_1 and ω_2 and between ω_3 and ω_4. The FID and the echo sequences were applied after this preparation step.

Figure 9(a) shows the Raman FID decay. The inset gathers the FT signal of the beatnote amplitude for different values of the delay. The FID lifetime is derived from the exponential decay of the maximum FT peak as function of T. T is increased by step of 1 μs from 1 to 16 μs. For each value of T, the amplitude of the beatnote is averaged over 40 measurements and the experiments are repeated three times. We found $T^*_{2,\mathrm{Raman}}=5.6\pm0.2$ μs which gives a $\Gamma^*_{2,\mathrm{Raman}}=57\pm2$ kHz. Figure 9(b) gathers the Raman echo signal decay with the FT intensity of the beatnote in the inset. T is increased by step of 10 μs from 10 to 240 μs. Two decays can be seen on Fig. 9(b), a fast one in the 0–30 μs time range which corresponds to the contribution of the FID of the second bichromatic pulse, and a long one in the 40–240 μs time range due to the Raman echo decay. An exponential fit of this last decay in the 40–240 μs range gives a value of $T_{2,\mathrm{Raman}}=250\pm15$ μs which implies $\Gamma_{\mathrm{Raman}}=1.25\pm0.1$ kHz. As we can see from the experimental data, an increase of the Raman intensity is observed between 100 and 150 μs. This increase is reproducible and it could come from modulations due to superhyperfine splittings caused by interactions with the W nuclei.

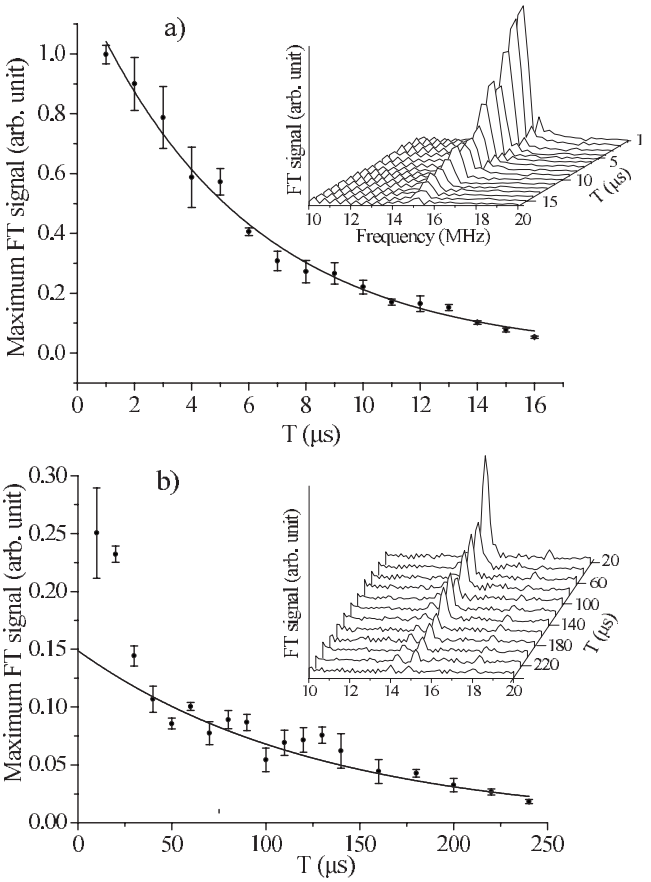

FIG. 9. (a) FID decay as function of the delay T between the first pulse and the read-out pulse. The inset gathers the FT signal linked to the beatnote amplitude for different values of the delay. An exponential fit (solid line) of the decay gives $T^*_{2,\mathrm{Raman}}=5.6\pm0.2$ μs. (b) Raman echo decay as a function of the delay T between the first pulse and the second bichromatic pulse, with an inset that gathers the FT peak at δ_2^g for different values of T. Two decays can be seen on Fig. 9(b), a fast one in the 0–30 μs time range which corresponds to the contribution of the FID of the second bichromatic pulse, and a long one in the 40–240 μs time range due to the Raman echo decay. An exponential fit of this last decay in the 40–240 μs range gives a value of $T_{2,\mathrm{Raman}}=250\pm15$ μs.

VI. CONCLUSION

The hyperfine structure and hyperfine coherent properties of Pr^{3+} ions in single crystalline $La_2(WO_4)_3$ were studied by hole-burning and photon echo techniques. Different sequences of optical hole-burning pulses were used to reveal the individual hyperfine transitions. These sequences create a transparent region within the inhomogeneously broadened $^3H_4(0) \rightarrow {}^1D_2(0)$ absorption line by optical pumping and then burn-back ions with transitions within this region and finally isolate some specific transitions for only one class of Pr^{3+} ions by applying additional clean-wrong-class pulses. The ordering of the hyperfine splittings in the $^3H_4(0)$ ground state and in the $^1D_2(0)$ excited state was obtained. The relative and absolute oscillator strengths were determined by comparing the absorption on several transitions starting from a common lower level and by measuring Rabi flopping as the transitions were coherently driven.

The inhomogeneous and homogeneous hyperfine linewidths were obtained by free induction decay and Raman echo experiments. The hyperfine structure of Pr^{3+} ions, composed of three hyperfine levels for each electronic level, allowed a reliable measurement of these two parameters, as the FID and the Raman echo could be detected on optical transitions which were not excited by the optical coherent driving pulses.

Knowing the hyperfine splittings and the coherent hyperfine properties of Pr^{3+} ions in $La_2(WO_4)_3$, several three-level Λ systems can be defined in this new system and the spectroscopic data that was obtained in this work will be used in further experiments devoted to electromagnetically induced transparency, stopped light and quantum memory.

ACKNOWLEDGMENTS

The authors would like to acknowledge financial support by the EADS foundation, the Access to Research Infrastructures activity in the 6th Framework program of the EU (Contract No. RII3-CT-2003-506350, Laserlab Europe), the European Commission through the integrated project QAP, the Swedish Research Council and the Knut and Alice Wallenberg foundation

*Author to whom correspondence should be addressed; olivier-guillotn@enscp.fr

[1] J. I. Cirac, P. Zoller, H. J. Kimble, and H. Mabuchi, Phys. Rev. Lett. **78**, 3221 (1997).
[2] H. J. Briegel, W. Dür, J. I. Cirac, and P. Zoller, Phys. Rev. Lett. **81**, 5932 (1998).
[3] N. Sangouard, C. Simon, J. Minar, H. Zbinden, H. de Riedmatten, and N. Gisin, Phys. Rev. A **76**, 050301(R) (2007).
[4] B. Julsgaard, J. Sherson, J. I. Cirac, J. Fiurasek, and E. S. Polzik, Nature (London) **432**, 482 (2004).
[5] T. Chanelière, D. N. Matsukevich, S. D. Jenkins, S.-Y. Lan, T. A. B. Kennedy, and A. Kuzmich, Nature (London) **438**, 833 (2005).
[6] M. D. Eisaman, A. André, F. Massou, M. Fleischhauer, A. S. Zibrov, and M. D. Lukin, Nature (London) **438**, 837 (2005).
[7] D. F. Phillips, A. Fleischhauer, A. Mair, R. L. Walsworth, and M. D. Lukin, Phys. Rev. Lett. **86**, 783 (2001).
[8] A. V. Turukhin, V. S. Sudarshanam, M. S. Shahriar, J. A. Musser, B. S. Ham, and P. R. Hemmer, Phys. Rev. Lett. **88**, 023602 (2001).
[9] K. Ichimura, Opt. Commun. **196**, 119 (2001).
[10] N. Ohlsson, R. K. Mohan, and S. Kröll, Opt. Commun. **201**, 71 (2002).
[11] J. J. Longdell, E. Fraval, M. J. Sellars, and N. B. Manson, Phys. Rev. Lett. **95**, 063601 (2005).
[12] M. Nilsson and S. Kröll, Opt. Commun. **247**, 393 (2005).
[13] J. J. Longdell, A. L. Alexander, and M. J. Sellars, Phys. Rev. B **74**, 195101 (2006).
[14] R. M. Macfarlane, J. Lumin. **100**, 1 (2002).
[15] M. D. Lukin, Rev. Mod. Phys. **75**, 457 (2003).
[16] B. S. Ham, P. R. Hemmer, and M. S. Shariar, Opt. Commun. **144**, 227 (1997).
[17] J. Klein, F. Beil, and T. Halfmann, Phys. Rev. Lett. **99**, 113003 (2007).
[18] O. Guillot-Noël, Ph. Goldner, Y. Le Du, P. Loiseau, B. Julsgaard, L. Rippe, and S. Kröll, Phys. Rev. B **75**, 205110 (2007).
[19] X. Lin, Y. Chen, J. Liao, Z. Luo, and Y. Huang, J. Cryst. Growth **266**, 487 (2004).
[20] M. Gärtner, D. Abeln, A. Pring, M. Wilde, and A. Reller, J. Solid State Chem. **111**, 128 (1994).
[21] M. Nilsson, L. Rippe, N. Ohlsson, T. Christiansson, and S. Kröll, Phys. Scr., T **T102**, 178 (2002).
[22] M. Nilsson, L. Rippe, S. Kroll, R. Klieber, and D. Suter, Phys. Rev. B **70**, 214116 (2004); **71**, 149902(E) (2005).
[23] L. Rippe, M. Nilsson, S. Kröll, R. Klieber, and D. Suter, Phys. Rev. A **71**, 062328 (2005).
[24] M. S. Silver, R. I. Joseph, and D. I. Hoult, Phys. Rev. A **31**, 2753 (1985).
[25] I. Roos and K. Molmer, Phys. Rev. A **69**, 022321 (2004).
[26] F. de Seze, F. Dahes, V. Crozatier, I. Lorgeré, F. Bretenaker, and J. L. Le Gouët, Eur. Phys. J. D **33**, 343 (2005).
[27] M. A. Teplov, Zh. Eksp. Teor. Fiz. **53**, 1510 (1967) [Sov. Phys. JETP **26**, 872 (1968)].
[28] R. M. Macfarlane and R. M. Shelby, in *Spectroscopy of Solids Containing Rare Earth Ions*, edited by A. A. Kaplyanskii and R. M. Macfarlane (North Holland, Amsterdam, 1987), p. 51.
[29] J. J. Longdell, M. J. Sellars, and N. B. Manson, Phys. Rev. B **66**, 035101 (2002).
[30] Ph. Goldner and O. Guillot-Noël, Opt. Mater. **28**, 21 (2006).